FACTA UNIVERSITATIS
Series: **Mechanical Engineering**
https://doi.org/10.22190/FUME241212009A

Original scientific paper

NUMERICAL MODELLING OF THE CROSSWIND INFLUENCE ON VEHICLE AERODYNAMICS IN HIGHWAY TRAFFIC CONDITIONS

Daniela Alic[1], Jonas Matijošius[2], Artūras Kilikevičius[2]

[1]Politehnica University Timisoara, Faculty of Engineering Hunedoara, Romania
[2]Vilnius Gediminas Technical University, Mechanical Science Institute, Lithuania

Abstract. *This study presents an efficient numerical model for evaluating the impact of crosswinds on vehicle aerodynamics using ANSYS Fluid Flow. It offers valuable insights into the qualitative behavior of vehicles under typical highway traffic conditions. The analysis explores airflow distribution when a car overtakes a truck at approximately 100 km/h, considering weak, moderate, and strong lateral winds. A detailed examination of the overtaking phases, with vehicles positioned in three distinct configurations, reveals significant aerodynamic interactions. These interactions influence vehicle handling and stability, as reflected in variations in velocity and pressure distributions, increased drag coefficients for the truck under stronger lateral winds, and significant fluctuations in the car's drag coefficients based on its position relative to the truck. Additionally, Reynolds numbers indicate a transition to turbulent flow. This paper provides an in-depth analysis and discussion of these findings.*

Key words: *Aerodynamic analysis, Passing maneuvers, Crosswind, Computational fluid dynamics, Drag and lift coefficients, Reynolds Number*

1. INTRODUCTION

In recent years, the study of vehicle aerodynamics has gained increasing attention, particularly due to the growing emphasis on energy efficiency, sustainability, and safety in transportation systems. Aerodynamic drag coefficients are a critical factor influencing the energy consumption of vehicles, especially at highway speeds, where air resistance constitutes a significant portion of the overall drag force. A detailed understanding of the factors that contribute to aerodynamic drag, such as vehicle design, speed, environmental and traffic conditions, is essential for optimizing fuel efficiency and reducing emissions

Received: December 12, 2024 / Accepted February 28, 2025
Corresponding author: Daniela Alic
Politehnica University Timisoara, Faculty of Engineering Hunedoara, Revolutiei Str. 5, Hunedoara, Romania
E-mail: daniela.alic@upt.ro

[1]. Among these factors, the impact of crosswinds on aerodynamic performance has emerged as a significant area of interest [2].

Crosswinds, acting perpendicularly to the direction of travel, can dramatically alter the aerodynamic forces experienced by vehicles. On highways, where vehicles travel at high speeds and in close proximity to one another, crosswinds not only increase the drag force but also affect vehicle stability and driver control [3]. The interaction between vehicles under crosswind conditions introduces additional complexity, as aerodynamic wake effects and interference between vehicles can amplify drag forces and influence the vehicle's lateral dynamics. Consequently, understanding the effect of crosswind on the vehicle interaction on highways is critical for improving both fuel efficiency and safety.

Numerical modeling plays a key role in analyzing the influence of crosswinds on vehicle aerodynamics. Through extensive computational fluid dynamics (CFD) simulations, researchers can evaluate the complex flow patterns and pressure distributions that arise when crosswinds interact with multiple vehicles [4], as well as the Truck-Induced Wind Gusts [5], that may affect the resilience and safety of highway traffic signals structures. Numerical models allow for detailed analysis of various parameters, such as vehicle spacing, crosswind speed, and vehicle geometry, without the need for extensive physical testing. These simulations offer valuable insights into the effect of crosswind conditions on the aerodynamic drag, especially in scenarios involving multiple vehicles traveling in close formation, such as convoys, in platoon [6], or during overtaking maneuvers [7].

The motivation for conducting numerical modeling of crosswind effects lies in the potential benefits for both vehicle design and transportation planning. By reducing aerodynamic drag through optimized vehicle shapes and logistic transportation configurations, manufacturers can improve vehicle fuel efficiency, resulting in lower operating costs and reduced greenhouse gas emissions. Furthermore, understanding the impact of crosswinds on vehicle dynamics contributes to highway safety by guiding vehicle control strategies and enhancing driver assistance systems, particularly in regions prone to strong crosswinds. This study aims to investigate the effects of crosswinds on the aerodynamic drag generated by vehicle interaction on highways through numerical modeling. By providing a detailed analysis of drag variations under different crosswind conditions, this research seeks to contribute to the development of more energy-efficient and safer vehicle designs, as well as strategies for mitigating the adverse effects of crosswinds on highways traffic.

2. Theoretical Basis and Numerical Setup

The numerical modeling of crosswind influence on air drag from vehicle interaction on highways relies on a strong theoretical foundation rooted in fluid dynamics, aerodynamics, and computational methods [8]. In the context of Computational Fluid Dynamics (CFD) simulations using ANSYS software, several fundamental principles and mathematical models are employed to accurately represent the complex flow behaviors encountered in vehicle aerodynamics under crosswind conditions [9].

The core theoretical framework for modeling airflow in CFD, based on the Navier-Stokes equations, describes the motion of fluid substances. These equations are a coupled set of nonlinear partial differential equations for five unknowns: three velocity components and two state variables (pressure, density or energy), which are connected by an equation

of state. These account for the conservation of mass (continuity equation), momentum (Newton's second law), and energy (first law of thermodynamics) [10].

Our numerical model employs a viscous Shear Stress Transport (SST) k-ω model, a widely used two-equation eddy-viscosity turbulence framework that serves as an approximation for the Reynolds-averaged Navier–Stokes (RANS) equations and has proven to provide results that match well with experimental data [11]. In the RANS approach, equations are solved for the time-averaged flow characteristics while capturing the scale of turbulent fluctuations. The time average is defined as

$$\bar{f} = \lim_{T\to\infty} \frac{1}{T} \int_0^T f(x_i, t)\, dt \tag{1}$$

and the instantaneous field flow is represented as $u_i = \bar{u}_i + \acute{u}_i$, namely the sum of a time-mean component and a fluctuating component.

Averaging the Navier–Stokes equations yields the RANS equations [12], which contain the Reynolds stress tensor $-\rho\, \overline{\acute{u}_\iota \acute{u}_j}$ as a key term representing the averaged effects of turbulent convection. RANS models are classified into two main categories based on how this stress tensor is computed: Eddy viscosity models, which assume that stress is proportional to strain (velocity gradients) and incorporate an effective turbulent viscosity, and Reynolds stress models**,** which provide a more detailed representation of the stress tensor without the assumption of proportionality to strain. Eddy viscosity, similar in effect to molecular viscosity, facilitates the diffusion of momentum. Unlike molecular viscosity, it is not an inherent fluid property but rather a characteristic of turbulent flow.

Turbulence is characterized by random, instantaneous fluctuations in both space and time. However, statistical averaging of these fluctuations reveals measurable transport mechanisms. The turbulent kinetic energy (k) equation is used to define the turbulence velocity scale:

$$\frac{\partial(\rho\, k)}{\partial t} + \frac{\partial(\rho\, \bar{u}_j\, k)}{\partial x_j} = -\rho\, \overline{\acute{u}_\iota \acute{u}_j} \frac{\partial \bar{u}_j}{\partial x_j} - \rho\varepsilon + \frac{\partial}{\partial x_j}\left[\frac{\partial k}{\partial x_j}\left(\mu + \frac{\mu_t}{\sigma_k}\right)\right] \tag{2}$$

where the first term on the right-hand-side represents the rate of production of turbulent kinetic energy, P_k, driven by mean flow gradients, and ε denotes the dissipation rate, describing the conversion of kinetic energy into internal energy due to viscous effects. Physically, turbulent kinetic energy is produced due to the mean flow gradients, and is dissipated by viscous effects. Imbalance between the production and the dissipation will cause k either to grow or to decay. The final term is a diffusion term, typically modeled using the gradient diffusion hypothesis or Reynolds analogy, which introduces the turbulent Prandtl number to quantify turbulent diffusion effects.

The motivation behind two-equation models originates from the need to obtain the two scales required to compute the eddy-viscosity. Based on dimensional arguments, a length-scale and a time-scale are required for that purpose. The standard k-ω model is a two-equation turbulence model that solves transport equations for k and ω (specific dissipation rate, ε/k). This model excels in simulating wall-bounded boundary layers, free shear flows, and low Reynolds number flows. It is particularly effective for complex boundary layer flows under adverse pressure gradients, separation (as in external aerodynamics), and transitional flows.

The SST k-ω model is an enhanced version of the standard k-ω model, combining the strengths of both the original k-ω approach for near-wall regions and the k-ε model for regions farther from the wall. The corresponding equations are:

$$\frac{\partial(\rho\, k)}{\partial t} + \frac{\partial(\rho\, \bar{u}_j\, k)}{\partial x_j} = P_k - C_\mu \rho k\omega + \frac{\partial}{\partial x_j}\left[\left(\mu + \frac{\mu_t}{\sigma_k}\right)\frac{\partial k}{\partial x_j}\right] \tag{3}$$

$$\frac{\partial(\rho\, \omega)}{\partial t} + \frac{\partial(\rho\, \bar{u}_j\, \omega)}{\partial x_j} = C_{\omega_1}\frac{\omega}{k}P_k - C_{\omega_2}\rho\omega^2 + \rho(1-F_1)CD + \frac{\partial}{\partial x_j}\left[\left(\mu + \frac{\mu_t}{\sigma_k}\right)\frac{\partial \omega}{\partial x_j}\right] \tag{4}$$

with the coefficients set in ANSYS as: $\mu_t = \rho\frac{k}{\max\left(\omega, \frac{F_2 S}{a_1}\right)}$, $CD = \frac{2}{\sigma_\omega}\frac{1}{\omega}\frac{\partial k}{\partial x_j}\frac{\partial \omega}{\partial x_j}$

$$C_{\omega_1} = \frac{5}{9}\,;\; C_{\omega_2} = \frac{3}{40}\,;\sigma_k = 1/0.85\,;\; \sigma_\omega = 2\,;\; C_\mu = 0.09\,;\; a_1 = 0.31$$

The standard k-ε model performs well in free-stream fully turbulent regions but struggles with complex flows involving severe pressure gradients, separation, or strong streamline curvature. The SST hybrid model addresses these limitations by employing a blending function F_1 that transitions smoothly between the k-ω model near walls and the k-ε model in high-Reynolds-number regions [12]. Additionally, it incorporates a modified turbulent viscosity formulation to account for the transport effects of primary turbulent shear stress, enhancing its accuracy in capturing complex flow behaviors.

The governing equations are discretized using the Finite Volume Method and Least Squares Cell-Based gradient evaluation [13]. As solution methods, a Coupled Scheme is employed for Pressure-Velocity Coupling, utilizing a Rhie-Chow momentum-based flux approach [14]. This method provides a robust and efficient single-phase implementation for steady-state flows, offering better performance than segregated solution schemes. To improve the accuracy of the simulation and better capture the turbulent flow over the vehicles, second-order upwind schemes are applied to the Turbulent Kinetic Energy and Specific Dissipation Rate. Additionally, the External-Aero Favorable Settings option is used during the Hybrid initialization phase to generate a more accurate initial velocity field for external-aero simulations. The volume mesh consists of poly-hexcore elements, with local refinement regions around the vehicles, as part of the standard Ansys Fluent Meshing watertight geometry workflow. Convergence verification is conducted by tracking the continuity equation, velocity components, and the k and ω values, ensuring that the solution residues decrease below 10^{-4} as convergence criterion.

3. NUMERICAL ANALYSIS

3.1 Numerical Modeling

Numerical modeling with specialized Computational Fluid Dynamics (CFD) software, such as ANSYS Fluent, is currently used for a wide range of applications in the automotive sector, due to its advanced physics modeling and industry leading accuracy [15]. Fluent is one of the two computational fluid dynamics (CFD) packages included with the ANSYS computational mechanical software suite. With increased traffic and advancements in technologies aimed at improving road safety, various driving scenarios are being analyzed

to assess aerodynamic drag coefficients (which impact fuel consumption), determine optimal vehicle spacing, and ensure safe travel under diverse conditions.

As one vehicle overtakes another, the airflow fields around both vehicles interact, generating transient aerodynamic forces that can adversely affect handling and stability. Sudden changes in airflow velocity within a vehicle's wake may cause abrupt variations in the aerodynamic forces acting on the overtaking vehicle. These rapid fluctuations can compromise control, making steering more challenging and increasing the risk of accidents. Understanding how light vehicles respond to disturbances caused by larger, heavier vehicles remains a complex challenge. This study investigates the impact of these aerodynamic disturbances on a passenger car when passing a large truck.

The car geometry is that of a BMW 1 Series [16], namely 4.3 m length, 1.8 m width and 1.43 m height. The truck with the streamlined geometry of a European truck [17] has a length of 10.5 m, width of 2.5 m and height of 4 m. The distance between the vehicles is 1.5 m on the z direction (Fig. 1).

The vehicles have a speed of 28 m/s (approximately 100 km/h), modeled through an airflow entering the front inlet boundary and flowing in the positive x direction (Fig. 1). The velocity of the lateral wind, entering the right inlet boundary and flowing in the positive z direction, is varied from 5 m/s, to 10 m/s and 15 m/s corresponding to weak, significant, respectively strong wind. This approach assumes that the relative velocity of the vehicles has a negligible effect on the flow distribution. The fluid is air, with density 1.225 kg/m^3 and viscosity 1.7894x10^{-05} kg/ms. The turbulent intensity, expressed by the percentage ratio of the flow rate variation with respect to the average flow rate, is set to 1%, while the turbulent viscosity ratio is set to 2 at the boundaries.

The interaction between the vehicles is modeled in three traffic phases. As the truck runs on the first lane, the car runs on the second lane and their dynamics is studied in the following phases: car behind the truck (Fig. 1a), parallel with the truck (Fig. 1b) and eventually in front of the truck (Fig. 1c).

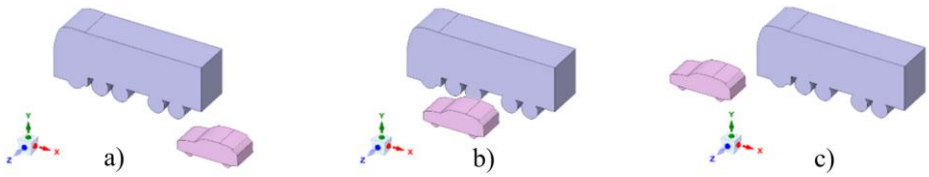

Fig. 1 Interaction between vehicles in 3 phases: a) car behind truck, b) car parallel with the truck, c) car in front of the truck

The numerical simulation domain consists of a box of 50 m length, 40 m width and 24 m height. The boundaries are set up as velocity-inlets: front yz boundary (flow in +x direction) and right yx boundary (flow in +z direction); pressure outlets: back yz boundary and left yx boundary; stationary shear zero wall: top xz boundary; moving no-slip wall: ground xz boundary; stationary no-slip walls: car and truck surfaces. In viscous fluids, the flow velocity at solid surfaces is zero relative to the boundary, which accounts for the no-slip condition. This condition is based on the physical observation that at the wall, the adhesive force of attraction between fluid and solid particles is stronger than the cohesive force between the fluid particles.

3.2 Numerical Results, Interpretations and Discussions

Our primary goal is to analyze airflow velocity vectors around vehicle bodies in the three cases, with Fig. 2 showing their top view in the xz plane for the first traffic phase.

a)

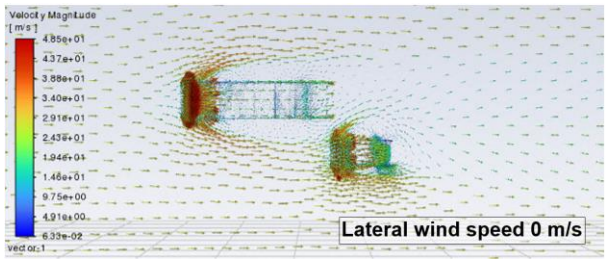

Drag coeff.
Truck x = 0.78
Car x = 0.45
Truck z = -0.02
Car z = -0.05

Lift coeff.
Car = 0.11

b)

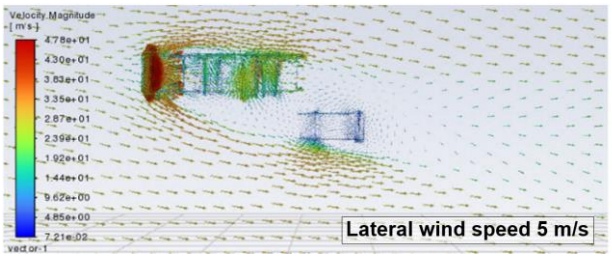

Drag coeff.
Truck x = 1.02
Car x = -0.17
Truck z = 0.15
Car z = -0.04

Lift coeff.
Car = -0.02

c)

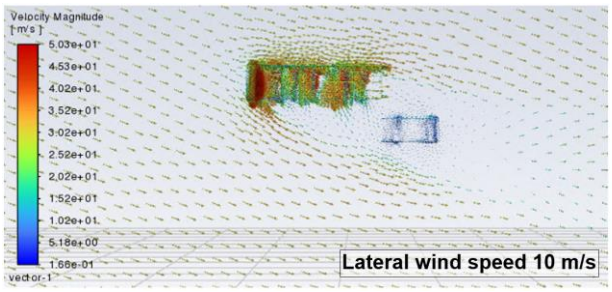

Drag coeff.
Truck x = 1.18
Car x = -0.19
Truck z = 0.35
Car z = -0.05

Lift coeff.
Car = -0.01

d)

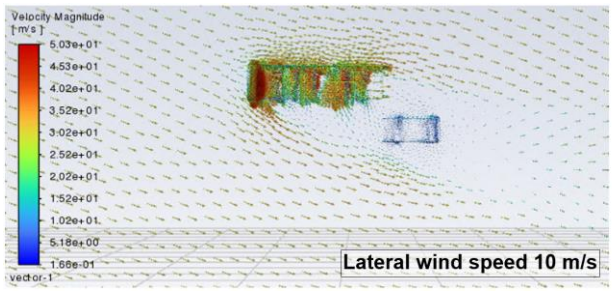

Drag coeff.
Truck x = 1.18
Car x = -0.19
Truck z = 0.35
Car z = -0.05

Lift coeff.
Car = -0.01

Fig. 2 Distribution and magnitude of the induced airflow velocity vectors and the related magnitude of drag and lift coefficients in Phase 1, at different lateral wind speeds

In the case with no lateral wind, illustrated in Fig. 2a, the typical airflow distribution around both vehicles is visible, with only a slight distortion in the x direction due to the interaction of their air currents as they travel in parallel lanes.

As lateral wind velocity increases (Fig. 2bcd) the main airflow behaves differently, with the truck acting as a lateral shield for the car, creating an area of low airflow velocity around the car. The drag coefficient values confirm this, indicating a reduction in drag on the car in the x direction, making its movement easier despite the increasing lateral wind, as the truck reduces its exposure to the airflow.

In the z direction, the drag on the car is minimal and directed towards the truck (showing negative values), suggesting a slight push of the car towards the truck. Meanwhile, the airflow velocity over the truck increases with lateral wind, reaching maximum values which exceed 1 (see discussion at the end of the section and reference [18]), not only in the front windshield area but also along the exposed sides and top of the truck body. This results in higher drag forces in both the x and z directions, indicating that the truck is being pushed backward and toward the car.

The Reynolds number of the induced airflow is plotted in Fig. 3, providing a top view of the xz plane. In the case of zero lateral wind (Fig. 3a), the plot shows laminar flow over the vehicles ($Re < 10^5$) and transitional flow in the wake of the truck. With increasing lateral wind, the airflow pattern changes significantly, showing higher Reynolds numbers, up to 1.25×10^6 , in transition to turbulent flow, not only in the rear of the truck but also around the car, as the left side of the truck airflow is largely diverted over the car.

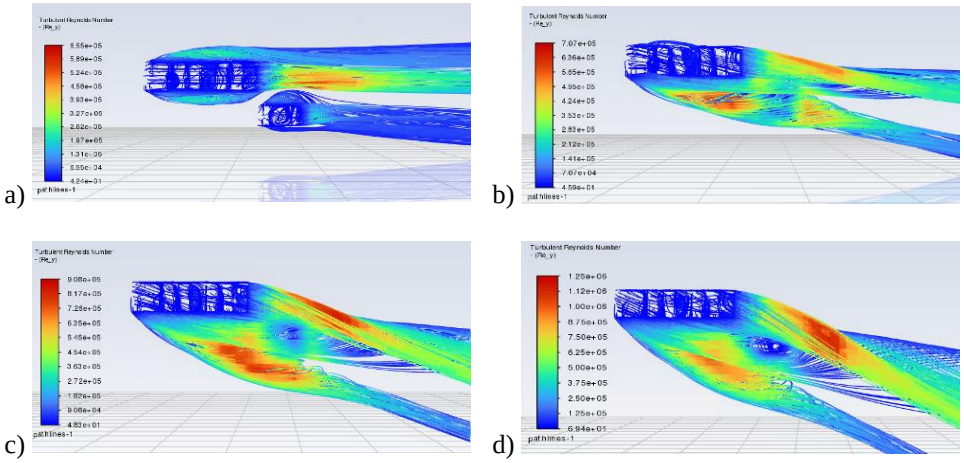

Fig. 3 Path lines of the induced airflow turbulence and magnitude of the Reynolds number in Phase 1, at lateral wind of: a) 0 m/s, b) 5 m/s, c) 10 m/s, d) 15 m/s

In the second phase of our study, the vehicles travel side by side. A comparison between the zero lateral wind scenarios in phases 1 and 2 reveals a slight increase in the car's drag coefficients along the x direction (Figs. 2a and 4a), as some of the airflow separating from the truck's windshield now reaches the car's windshield, raising the pressure. However, as lateral wind increases, the car's drag in the x direction decreases, since the truck disrupts both the frontal and lateral airflows, redirecting them almost tangentially to the car

(Fig.4bcd). This creates a partial shielding effect, reducing its drag. In the z direction, drag on the car increases, pushing it away from the truck.

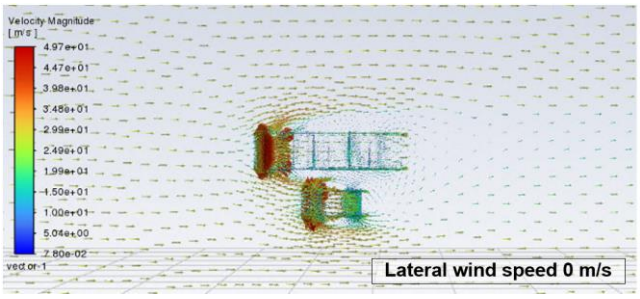

a) **Drag coeff.**
Truck x = 0.76
Car x = 0.53
Truck z = 0.0
Car z = 0.01

Lift coeff.
Car = 0.19

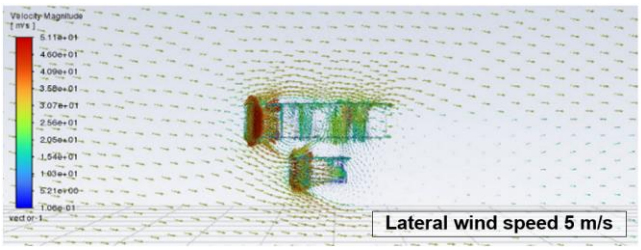

b) **Drag coeff.**
Truck x = 0.93
Car x = 0.39
Truck z = 0.19
Car z = 0.11

Lift coeff.
Car = 0.25

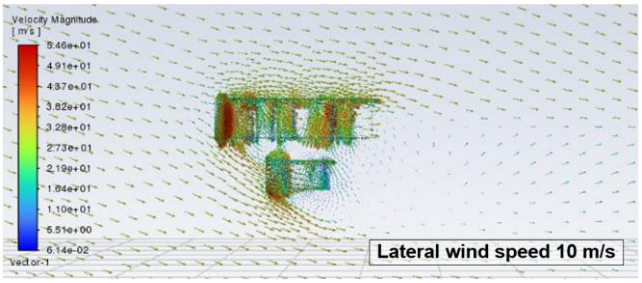

c) **Drag coeff.**
Truck x = 1.10
Car x = 0.31
Truck z = 0.40
Car z = 0.26

Lift coeff.
Car = 0.13

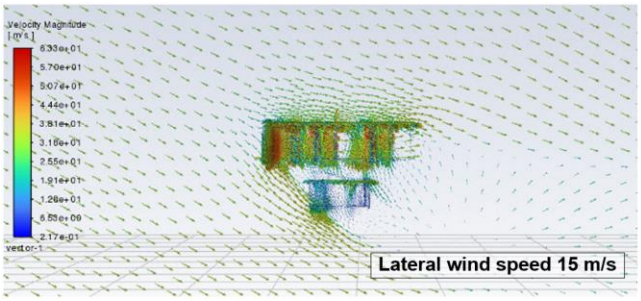

d) **Drag coeff.**
Truck x = 1.16
Car x = 0.06
Truck z = 0.55
Car z = 0.22

Lift coeff.
Car = 0.07

Fig. 4 Distribution and magnitude of the induced airflow velocity vectors and the related magnitude of drag and lift coefficients in Phase 2, at different lateral wind speeds

The Reynolds numbers (Fig. 5) indicate a similar pattern as analyzed for phase 1, with maxima around 10^6 in the wake of the truck and around its lateral region, where the separated airflow of the truck interacts with the surface of the car.

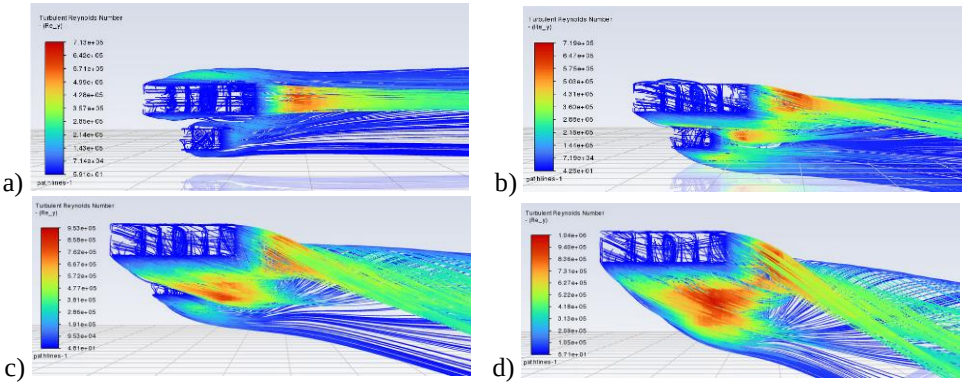

Fig. 5 Path lines of the induced airflow turbulence and magnitude of the Reynolds Number in Phase 2, at lateral wind of: a) 0 m/s, b) 5 m/s, c) 10 m/s, d) 15 m/s

In the third and final phase of our study, the car is fully exposed to both the frontal airflow and lateral wind (Fig. 6), resulting in a significant increase in car drag in both the x and z directions due to the higher wind velocity. The drag coefficients on the truck have similar values to phase 2, as its dynamics is not strongly influenced by the position of the car. However, the truck's influence on the car is obvious in all phases and still noticeable in phase 3, in the air velocity distribution formed in the wake of the car.

The airflow pattern is once again marked by Reynolds number peaks of 10^6 in the separated flow around the truck (Fig. 7), indicating a transitional flow that has not yet fully developed into turbulence (Re between 5×10^5 and 3×10^6). While accurate turbulence modeling is essential for predicting external vehicle flow - since higher Reynolds numbers suggest more intense turbulence, which can greatly increase drag - the results in this paper are produced using accessible computational resources and aim to provide an estimate of crosswind effects on the vehicle aerodynamics. A more detailed study of Reynolds numbers would be a valuable tool for optimizing aerodynamics, from evaluating different vehicle shapes to assessing specific design modifications such as spoilers and diffusers [19, 20].

In examining the cases with zero lateral wind velocity, it becomes clear that in all phases, the velocity plots show the airflow coming to a complete stop at the front of the vehicles before accelerating as it moves over the curved surfaces. This creates a high-pressure region at the front, which is more pronounced for the truck than for the car, where the air is deflected and flows along the aerodynamic surface. With lateral wind, this high-pressure region extends to the side of the truck, which provides a shielding effect for the car in phases 1 and 2. The main stagnation points remain on the front and lateral wind exposed surfaces where the airflow stops, then turns towards the edges and accelerates as it follows the vehicle contours. At the rear, the flow separates, leading to the formation of a recirculation region (wake). Due to the sharp change in the truck's surface shape and the

high Reynolds number, the flow separates abruptly, resulting in significantly larger separation regions compared to the car.

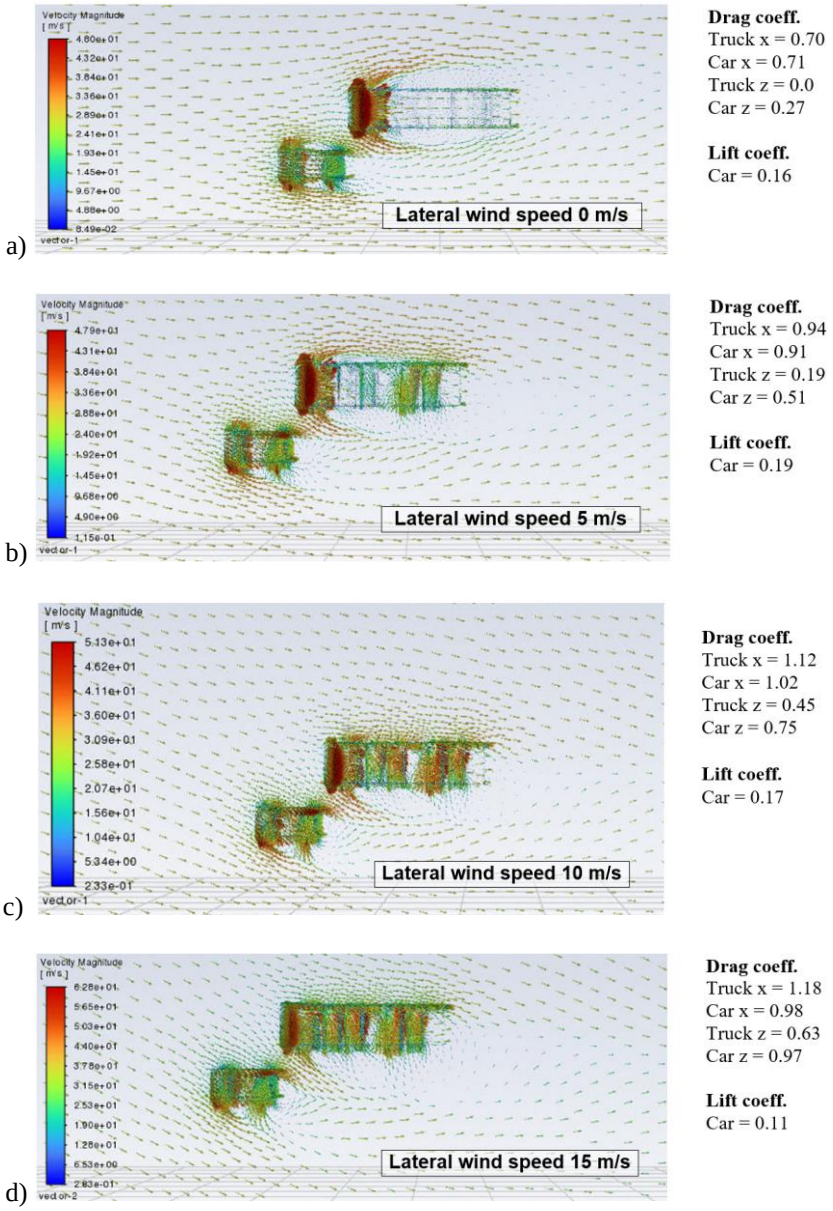

Fig. 6 Distribution and magnitude of the induced airflow velocity vectors and the related magnitude of the truck and car drag coefficients in Phase 3, at lateral wind of:
a) 0 m/s, b) 5 m/s, c) 10 m/s, d) 15 m/s

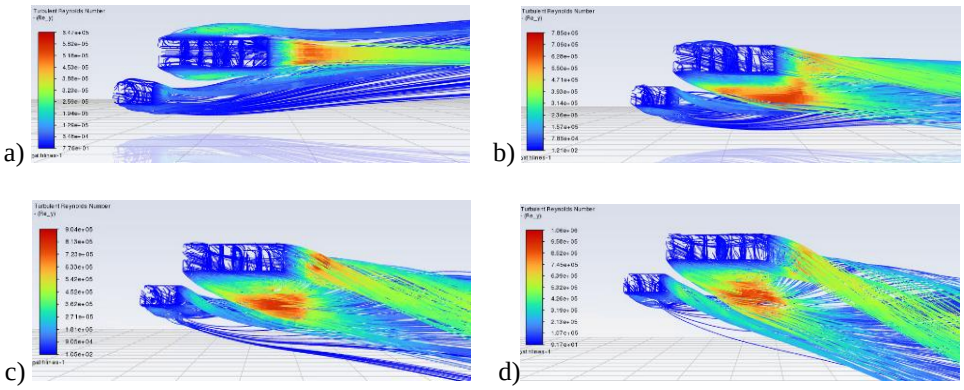

Fig. 7 Path lines of the induced airflow turbulence and magnitude of the Reynolds Number in Phase 3, at lateral wind of: a) 0 m/s, b) 5 m/s, c) 10 m/s, d) 15 m/s

As the airflow separates on the front and lateral of the vehicles, it forms pockets of high pressure and low velocity, which contribute to the pressure drag on the vehicles. This results in a significant increase in drag coefficients in the presence of lateral wind. In crosswind conditions, the airflow around both the truck and the car becomes highly unstable and less streamlined. Normally, the airflow over the vehicles is relatively smooth, helping to maintain a lower drag coefficient. However, crosswinds introduce additional lateral forces that disrupt this airflow, which becomes highly disturbed and less efficient, increasing the resistance experienced by the vehicles. This increased resistance raises the drag coefficient, in some cases above one [18].

As the flow moves around the vehicles, it accelerates over their curved surfaces, leading to a reduction in pressure. The velocity and pressure distribution on the vehicles, along with the viscous shear, generate forces on the vehicles: the drag force acting in the direction of the airflow and a vertical force acting perpendicular to the flow. The lower pressure on top of the vehicles also creates a lifting effect.

When a vehicle encounters a crosswind, the airflow becomes uneven, disrupting the direct front-to-rear flow. This disruption leads to irregular pressure distributions on the vehicle's surfaces, which can alter the overall lift force. During phase 1, the truck shields the car from the crosswind, significantly reducing the lift on the car and generating downforce (Fig. 1bcd). In phase 2, the crosswind initially increases lift by creating a pressure unbalance between the side facing the wind and the protected side (Fig. 4b); however, as the angle of the crosswind shifts, the truck shields the car again, reducing lift (Fig. 4cd). In phase 3, the car is fully exposed to the crosswinds, experiencing an initial lift increase due to the pressure differential (Fig. 6bc), followed by a decrease as the pressure balances on the side of the car exposed to the lateral wind (Fig. 6d).

While much of the existing research has focused on the direct impact of aerodynamic forces on isolated vehicles [21, 22], the influence of crosswinds and vehicle interactions on highways remains an underexplored yet increasingly important area of study. Numerical modeling provides a powerful tool to investigate these complex aerodynamic phenomena, offering insights that are difficult to control and expensive to obtain through experimental methods alone.

4. CONCLUSIONS

In automotive engineering, accurately predicting and minimizing aerodynamic drag is essential for improving vehicle performance, fuel efficiency, and overall safety. Understanding the effects of crosswinds on vehicle interactions is crucial, as they directly influence both energy consumption and stability. Crosswinds can substantially alter aerodynamic forces, particularly in multi-vehicle scenarios such as close-proximity driving or highway overtaking maneuvers. These interactions can lead to rapid and large fluctuations in air drag coefficients, strongly affecting fuel efficiency, handling, and stability, and potentially compromising road safety.

Furthermore, with the advent of advanced driver-assistance systems (ADAS) and the future integration of autonomous vehicles, the ability to predict and mitigate adverse aerodynamic effects becomes even more important. Vehicles equipped with such technologies often operate in convoys or platoons, where crosswind-induced drag variations can lead to significant energy inefficiencies and control challenges. Thus, developing reliable numerical models that can accurately simulate these scenarios is essential for optimizing vehicle design and improving the safety and efficiency of highway transportation.

This study provides a comprehensive numerical analysis of crosswind effects on aerodynamic drag coefficients in vehicle interactions on highways. By leveraging advanced computational fluid dynamics techniques, we quantify the drag forces under varying crosswind conditions and vehicle interaction in real-traffic scenarios, where vehicles travel at high speeds and in close proximity. In such conditions, crosswinds can significantly impact vehicle stability and fuel consumption. Optimizing vehicle shapes and transportation configurations can help mitigate these aerodynamic challenges, leading to safer and more energy-efficient designs, and improved traffic management under adverse environmental conditions. Furthermore, our approach contributes to strategies for minimizing the adverse effects of crosswinds, offering guidance on setting appropriate highway speed limits in moderate to strong wind conditions, ultimately enhancing both safety and efficiency.

Future work will focus on exploring a broader range of vehicles and configurations, as our current study is limited to a certain type of vehicles, representative for their class, which could provide deeper insights into crosswind effects. Additionally, we will investigate the impact of crosswinds on different vehicle formations under diverse environmental conditions. Another promising research direction involves integrating our findings into the development of advanced driver-assistance systems and autonomous vehicles.

REFERENCES

1. Ekman, P., 2020, *Important Factors for Accurate Scale-Resolving Simulations of Automotive Aerodynamics*, Dissertation Thesis, Linkoeping University, Sweden.
2. Askerdal, M., Fredriksson, J., Laine, L., 2023, *Development of simplified air drag models including crosswinds for commercial heavy vehicle combinations*, Vehicle System Dynamics, 62(5), pp. 1085-1102.
3. Pasala, K., Bhargav, A., Jeevan Rao, H., Sreenath Reddy, K., Seshaiah Naidu, T.V., 2014, *A CFD Investigation into the flow distribution on a car passing by a truck*, International Journal of Current Engineering and Technology, 2(2), pp. 525-528.
4. Van, D.D., Chou, C.C., Chang, K.C., 2022, *Aspects on numerical simulation of overtaking process between two vehicles*, Journal of Aeronautics, Astronautics and Aviation, 54(2), pp. 161-178.

5. Alic, D., Miltenovic, A., Banic, M., Zafra, R.V., 2025, *Numerical investigation of large vehicle aerodynamics under the influence of crosswind*, Spectrum of Mechanical Engineering and Operational Research, 2(1), pp. 13-23.
6. Scurtu, I.L., Gheres, M.I., 2022, *Numerical evaluation of vehicles aerodynamics in platoon using CFD simulation*, IOP Conf. Series: Materials Science and Engineering, 1220, 012024.
7. Van, D.D., Chou, C.C., Chang, K.C., 2023, *Numerical and experimental study of two-vehicle overtaking process*, Advances in Mechanical Engineering, 15(12), https://doi.org/10.1177/16878132231221044.
8. Tsubokura, M., Kobayashi, T., Nakashima, T., Nouzawa, T., Nakamura, T., Zhang, H., Onishi, K., Oshima, N., 2009, *Computational visualization of unsteady flow around vehicles using high performance computing*, Computes & Fluids, 38(5), pp. 981-990.
9. Bodhisagar, J.T., Bajaj, P.S., 2022, *A review on the effect of aerodynamics on car overtaking truck using CFD analysis method*, International Research Journal of Engineering and Technology, 9(8), pp. 1273-1279.
10. https://www.ansys.com/academic/educators/education-resources/teaching-package-governing-equations-of-fluids (last access: 12.03.2025)
11. Fike, M., Predin, A., Hren, G., Pezdevsek, M., 2024, *Analytical, numerical and experimental performance prediction of a model-sized wind turbine*, Technical Gazette, 31(2), pp. 612-617.
12. https://www.ansys.com/content/dam/amp/2022/march/quick-request/Best%20Practice%20RANS%20Turbulence%20Modeling%20in%20Ansys%20CFD.pdf (last access: 12.03.2025)
13. https://www.afs.enea.it/project/neptunius/docs/fluent/html/th/node368.htm (last access: 12.03.2025)
14. https://www.afs.enea.it/project/neptunius/docs/fluent/html/th/node373.htm (last access: 12.03.2025)
15. Varadarajoo, P.K., Ishak, I.A., Maji, D.S.B., Maruai, N.M., Khalid, A., Mohamed, N., 2022, *Aerodynamic analysis on the effects of frontal deflector on a truck by using Ansys software*, International Journal of Integrated Engineering, 14(6), pp.77-87.
16. https://www.bmw.com.sg/en/all-models/1-series/bmw-1-series/bmw-1-series-technical-data.html/bmw-116.bmw (last access: 12.03.2025)
17. https://3dmodels.org/3d-models/mercedes-benz-actros-tractor-3-axis-2011/ (last access: 12.03.2025)
18. Shao, N., Yao, G., Zhang, C., Wang, M., 2017, *A research into the flow and vortex structures around vehicles during overtaking maneuver with lift force included*, Advances in Mechanical Engineering, 9(9), https://doi.org/10.1177/1687814017732892.
19. Zhang, C., Bounds, C.P., Foster, L., Uddin, M., 2019, *Turbulence modeling effects on the CFD predictions of flow over a detailed full-scale sedan vehicle*, Fluids, 4(3), 148, https://doi.org/10.3390/fluids4030148.
20. Gu, Y., Liu, Y., Shen J., Wang, D., 2023, *Optimization of Reynolds number's effects on aerodynamic drag and automotive performance*, Theoretical and Natural Science, 13(1), pp.144-149.
21. Ghani, I.A., Hassan, R., Amin, I., Suhan, A., Husni, K., Didane, D.H., Manshoor, B., 2023, *Computational fluid dynamics (CFD) study on the aerodynamic of truck*, Journal of Design for Sustainable and Environment, 5(2), pp. 23-27.
22. Scurtu, I.S., 2021, *Aerodynamic performance evaluation for a vehicle structure equipped with a bicycle rack*, Automotive Engineering, 58, pp. 10-14.